Titre: Title:	Interactions between PLA, organo-montmorillonite and plasticizer: Synergistic effect on the barrier and mechanical properties of PLA nanocomposites blown films
Auteurs: Authors:	Salima Adrar, & Abdellah Ajji
Date:	2023
Type:	Article de revue / Article
Référence: Citation:	Adrar, S., & Ajji, A. (2023). Interactions between PLA, organo-montmorillonite and plasticizer: Synergistic effect on the barrier and mechanical properties of PLA nanocomposites blown films. Journal of Applied Polymer Science, 54867 (16 pages). https://doi.org/10.1002/app.54867

Document en libre accès dans PolyPublie
Open Access document in PolyPublie

URL de PolyPublie: PolyPublie URL:	https://publications.polymtl.ca/56711/
Version:	Version officielle de l'éditeur / Published version Révisé par les pairs / Refereed
Conditions d'utilisation: Terms of Use:	CC BY-NC-ND

Document publié chez l'éditeur officiel
Document issued by the official publisher

Titre de la revue: Journal Title:	Journal of Applied Polymer Science
Maison d'édition: Publisher:	Wiley
URL officiel: Official URL:	https://doi.org/10.1002/app.54867
Mention légale: Legal notice:	This is an open access article under the terms of the Creative Commons Attribution-NonCommercial-NoDerivs License, which permits use and distribution in any medium, provided the original work is properly cited, the use is non-commercial and no modifications or adaptations are made.© 2023 The Authors.

RESEARCH ARTICLE

JOURNAL OF **Applied Polymer** SCIENCE WILEY

Interactions between PLA, organo-montmorillonite and plasticizer: Synergistic effect on the barrier and mechanical properties of PLA nanocomposites blown films

Salima Adrar [ORCID] | Abdellah Ajji

CREPEC, Département de génie chimique, Polytechnique Montréal, Montreal, Quebec, Canada

Correspondence
Abdellah Ajji, CREPEC, Département de génie chimique, Polytechnique Montréal, Montreal, QC, Canada.
Email: abdellah.ajji@polymtl.ca

Abstract

In this study, the impact of incorporating a plasticizer on the compatibility between organo-montmorillonite (OMMt) and polylactic acid (PLA) is investigated, and the resulting barrier and mechanical properties are reported. Four polymers were chosen as plasticizers to prepare the PLA nanocomposite blown films: poly(ethylene glycol), poly(ethylene oxide), polycaprolactone (PCL), and random ethylene-methyl acrylate-glycidyl methacrylate terpolymer. Firstly, 5 wt% of each plasticizer and 3 wt% of OMMt (Dellite® D43B) were mixed simultaneously with PLA in a twin-screw extruder and then introduced into the hopper of a single screw extruder to produce D43B-PLA/plasticizer nanocomposite films. The compatibilization effect was examined based on microstructure observations and thermodynamic predictions. Crystallinity was evaluated using DSC and XRD measurements. The results obtained for permeability and mechanical testing showed that the improvement of barrier and mechanical properties depends directly on the degree of compatibility between plasticizer, OMMt, and PLA. Indeed, the interfacial properties, XRD diffraction, and TEM images showed that a synergistic effect can result from high interfacial interactions between different compounds.

KEYWORDS
barrier properties, compatibility, mechanical properties, organo-montmorillonites, PLA, plasticizer

1 | INTRODUCTION

Biopolymers are considered as an alternative raw material for the development of compostable packaging with high performances.[1] Poly(lactic acid) is one of the biopolymers with the highest potential to produce compostable packaging generally intended to be used for short time applications such as food packaging.[2,3] This linear aliphatic polyester exhibits good heat sealability, excellent barrier to flavor, high clarity, etc. Nevertheless, its high stiffness makes it brittle and its poor barrier properties to gas limited its use in packaging field,[4,5] particularly in food sector. To broaden the application of PLA as efficient packaging, particularly in food industry, an improvement in terms of flexibility and barrier properties is necessarily.

To enhance the flexibility and elongation at break of polylactic acid (PLA), a biodegradable polymer, various strategies have been explored while preserving its compostable nature.[4-7] One approach involves copolymerization and blending with flexible polymers like poly (butylene succinate) (PBS). Alternatively, incorporating lower concentrations of other biodegradable polymers such as poly(butylene adipate-co-terephthalate) (PBAT) and polycaprolactone (PCL) has proven effective.[4,7,8] Furthermore, non-biodegradable but water-soluble polymers like poly(ethylene glycol) (PEG) and poly(ethylene oxide) (PEO) have been used to improve PLA's mechanical properties.[5,6,9] Additionally, materials such as acetyl tri-n-butyl citrate (ATBC) and ethylene-methyl acrylate-glycidyl methacrylate terpolymer have been employed as plasticizers to mitigate PLA's inherent brittleness, thus increasing its elongation at break.[9,10]

The incorporation of nanoparticles represents another effective method for enhancing both the mechanical and barrier properties of PLA.[11-14] Specifically, the addition of nanoparticles, with a particular focus on organo-montmorillonites (OMMt), has been shown to improve the tensile modulus while reducing the elongation at break, especially at higher OMMt concentrations.[12] The impact of OMMt on PLA's permeability to gases and water varies depending on the specific type of OMMt used and its compatibility with the PLA matrix. Favorable interactions between OMMt and the PLA matrix can enhance the barrier properties of PLA by increasing its crystallinity or creating a tortuous path for diffusing molecules, facilitated by uniform dispersion within the matrix.[15,16]

Recent research has been focused on enhancing the mechanical strength, flexibility, and gas resistance of materials by leveraging the synergy between poly(lactic acid) (PLA), plasticizers, and nanofillers. Mohapatra et al. (2013) work demonstrated that incorporating PEG improved ductility but reduced tensile strength and modulus. Conversely, the addition of nanoclays, particularly C30B nanoclay at 3 wt%, improved both the tensile and impact properties.[17] In another study, a bio-based material consisting of PLA and PHB blends, plasticized with tributyrin (TB) and incorporating chitin nanoparticles (ChNPs), exhibited enhanced gas barrier properties, but suffered reduced ductility due to poor interfacial adhesion.[18] Additionally, nanocomposite films combining PBS and PLA with lamellar nanosilicate (Cloisite 30B) demonstrated superior oxygen barrier properties (+33%) and mechanical performance (+29% strain at break, +21% stress at break) when nanoparticles were selectively placed at the PBS/PLA interface.[19] It was also reported that blending PLA and PBAT with various clays and a polymeric epoxy-based chain extender plasticizer, results a bio-blend films with a significantly improved mechanical strength and barrier properties compared to PE films. The most promising formulation consisted of 25% PLA, 75% PBAT, 1% plasticizer, and 3% high-purity sepiolite clay.[20]

In a previous study, the choice of OMMt significantly influenced the oxygen permeability of PLA nanocomposite films, highlighting the importance of dispersion and compatibility. Specifically, the D43B-PLA system exhibited a strong interaction, resulting in increased crystallinity and an impressive 60% reduction in oxygen permeability, underscoring the pivotal role of OMMt properties in achieving effective gas barrier properties for food packaging.[21]

Building on these insights, our current study aims to delve deeper into our understanding by examining the influence of various plasticizers on the interplay between Dellite® 43B (D43B) and PLA. Additionally, we investigate how these chosen plasticizers impact the barrier and mechanical properties of PLA nanocomposite blown films. Our careful selection of plasticizers, including PEG, PEO, PCL, and a random ethylene-methyl acrylate-glycidyl methacrylate terpolymer (AX89), plays a pivotal role in sculpting the film's distinct characteristics. To maintain the films' compostable nature, we uphold a consistent composition of 5 wt% plasticizer and 3 wt% D43B, forming a sturdy basis for assessing the compatibility and overall performance of these nanocomposite films.

2 | EXPERIMENTAL SECTION

2.1 | Materials

Poly(lactic acid) Ingeo 4043D (density 1.24 g·cm^{-3}) was supplied by NatureWorks (Blair, NE, USA). It is an amorphous grade, specific for film applications, with a molecular weight around 110.000 g·mol^{-1}. PEG with a molecular weight 35,000 g.mol^{-1}, and PEO with $M_v = 9,00,000$ g·mol^{-1} were purchased from sigma Aldrich Inc., Canada. PCL (Capa™ 6800), linear polyester derived from caprolactone monomer, was supplied from perstorp (California, USA), with a molecular weight around 80,000 g·mol^{-1}. Lotader AX 8900 (AX89) as a random ethylene-methyl acrylate-glycidyl methacrylate terpolymer was provided by Arkema Investment Co., Ltd (Pennsylvania, USA).

The Dellites® 43B (D43B) is an OMMt which was purchased from Laviosa Chimica Mineraria SpA (Italy). According to the supplier, natural bentonite was modified with Dimethyl benzylhydrogenated tallow ammonium to obtain D43B.

2.2 | Preparation of the samples

Before processing, different resins and D43B were dried to remove remaining moisture. PLA and D43B were dried at 80°C under vacuum for 8 and 12 h, respectively. For

TABLE 1 The composition and the nomenclature of D43B-PLA/plasticizer nanocomposites films.

	PLA (wt%)	D43B (wt%)	Plasticizer (wt%)
PLA	100	—	—
PLA/PEO	95	—	5
PLA/PEG			
PLA/PCL			
PLA/AX89			
D43B-PLA	97	3	—
D43B-PLA/PEO	92	3	5
D43B-PLA/PEG			
D43B-PLA/PCL			
D43B-PLA/AX89			

the plasticizers, the drying lasted overnight under vacuum at 40 C for PCL, and at 50 C for PEO, PEG and AX89.

Different D43-PLA/plasticizer nanocomposite films were prepared in two steps. Firstly, PLA was mixed simultaneous with 3 wt% of D43B and 5 wt% of each plasticizer (Table 1) inside a twin-screw extruder (Lerstritz ZSE-18HP-40D, Germany), using a constant speed of 82 rpm and a decreasing temperature profile: 190–190–185–180–175–170–165. Then, the pellets of D43B-PLA/plasticizer nanocomposites were dried under vacuum at 80°C for 6 h and introduced inside a single screw extruder (Labtech Engineering Extrusion Line) to produce the D43-PLA/plasticizer nanocomposites blown films. This extruder has a single screw with a diameter of 20 mm, $L/D = 30$, and a spiral flow die with a diameter of 50 mm and an opening of 1 mm. A constant screw rotation speed of 70 rpm and a decreasing temperature profile that started from 180°C in the feeding zone to 175°C in the compression zone were used. The temperature of the die was fixed at 170°C. The winding speed and amount of air in the bubble were adjusted to obtain films with thicknesses around 55 μm and a double width of 13 cm.

2.3 | Characterization

2.3.1 | Atomic force microscopy (AFM)

An AFM (model: ICON FASTSCAN, BRUKER, Santa Barbara, CA, USA) in a tapping mode with RTESPA probe $k = 42$ N/m was used to investigate the morphology of the PLA/plasticizer blown films with and without 3 wt% D43B. The samples were molded in epoxy and the cross-sectional area was microtomed at room temperature using an ultramicrotome Leica (model EMFC7, USA).

2.3.2 | Surface energy measurements and interfacial energies

Surface energy for the different polymers and D43B were determined from static contact angle measurements using a goniometer telescope, model 100 from the Ramé-Hart, Inc. company. The measurements were taken at room temperature (23 C), using three solvents, purified water, formamide, and diiodomethane. The conditions and the method used to prepare the samples were defined in a previous study released on the PLA/PBAT/Cloisite nanocomposites.[8] When the drop settles on the surface of the polymer, the contact angle is formed at triple point (Image in Figure 1) and the Young's equation (Equation 1) relates this angle to the surface energies of the three interfaces, solid–gas (γ_s), liquid–gas (γ_l), and solid–liquid (γ_{sl}). However, the surface energy for the solid–liquid (γ_{sl}) interface is not known in general and different interaction models have been developed to estimate it.

In this study, the Owens–Wendt geometric mean equation in its linear form (Equation 1) was used to obtain surfaces energies of solids. In this model, the surface energies of liquids and solids were separated into two components, dispersive γ_s^d and polar γ_s^p with: $\gamma_s = \gamma_s^p + \gamma_s^d$ and $\gamma_l = \gamma_l^p + \gamma_l^d$. A linear form of Equation 1 ($y = ax + b$) leads directly to the solid components, $a = \sqrt{\gamma_s^p}$ and $b = \sqrt{\gamma_s^d}$ (Figure 1).

$$\frac{\gamma_l \cdot (1 + \cos\theta)}{2 \cdot \sqrt{\gamma_l^d}} = \sqrt{\gamma_s^p} \cdot \sqrt{\frac{\gamma_l^p}{\gamma_l^d}} + \sqrt{\gamma_s^d}. \tag{1}$$

The values of γ_s, γ_s^p and γ_s^d obtained for each system were extrapolated to processing temperature 180°C, using the temperature coefficients for each component (Equations 2 and 3).[22]
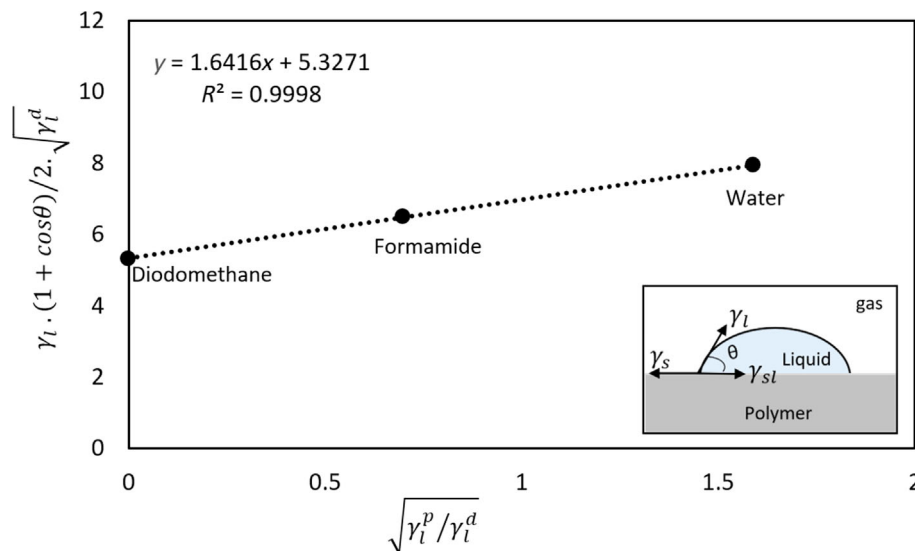
FIGURE 1 Owens–Wendt model: determination of the two components: dispersive γ_s^d and polar γ_s^p of polymers. [Color figure can be viewed at wileyonlinelibrary.com]

$$-d\gamma/dT = (11/9)(\gamma_0/T_c)(1 - T/T_C)^{2/9}, \quad (2)$$

$$\gamma = \gamma_0(1 - T/T_C)^{11/9}, \quad (3)$$

where γ_0 is the surface energy at 0 K, T_C is the critical temperature, and T is the temperature of the material in Kelvin. $-d\gamma/dT = 0.05$mN/m.°C for the polymer and $-d\gamma/dT = 0.1$mN/m.°C for nanoclay.[23] Then the interfacial energies were calculated using the geometric mean equation (Equation 4).

$$\gamma_{12} = \gamma_1 + \gamma_2 - 2\left[\sqrt{\gamma_1^d\gamma_2^d} + \sqrt{\gamma_1^p\gamma_2^p}\right]. \quad (4)$$

2.3.3 | The location thermodynamic prediction of D43B in the blends

In the thermodynamic equilibrium state, it is possible to predict the localization of D43B in the PLA/Plasticizer blends by determining the wetting parameter (ω_a) (Equation 5).[24] It depends on interfacial energies between PLA and plasticizers ($\gamma_{\text{PLA–Plasticizer}}$), and between that of OMMt and each of the two ($\gamma_{\text{D43B–PLA}}$; $\gamma_{\text{D43B–Plasticizer}}$).[4,7]

$$\omega_a = \frac{\gamma_{\text{D43B–PLA}} - \gamma_{\text{D43B–Plasticizer}}}{\gamma_{\text{PLA–Plasticizer}}}. \quad (5)$$

Hence, if $\omega_a > 1$, D43B will be located in the Plasticizer, while D43B will be inside PLA phase if $\omega_a < -1$. It is also possible to locate the D43B at the interface between PLA and Plasticizer, if $-1 < \omega_a < 1$.

In the literature, the localization of an OMMt in a polymer blends is generally associated with the presence

of an organic modifier (surfactant) at OMMt surface that can interact with polymer chains.[25] In order to evaluate the exact contribution of the surfactant on the localization of D43B in the PLA/plasticizers, another parameter was determined. The spreading coefficient, defined in the Equation 6, was used to estimate the localization of surfactant in the PLA/plasticizer blends.

$$\lambda_{abc} = \gamma_{ac} - (\gamma_{ab} + \gamma_{bc}), \quad (6)$$

where γ_{ac}, γ_{ab}, and γ_{bc} are the interfacial interactions between a and c, a and b, and between b and c; respectively. However, the values of the interfacial tensions between Surfactant (S43B) and each polymer were calculated using the Girifalco–Good equation (Equation 7).[9,10]

$$\gamma_{ab} = \gamma_a + \gamma_b - 2\phi(\gamma_a\gamma_b)^{1/2}, \quad (7)$$

where γ_{ab}, γ_a, and γ_b are the interfacial energy, surface energy of material **a**, and surface energy of material **b**, respectively. ϕ is a constant depending on the free energies of **a** and **b** materials. $\phi = 1$ can be used for making rough predictions of interfacial tensions for such blends with a fair degree of confidence.[9–11]

2.3.4 | Transmission electron microscopy (TEM)

Transmission electron microscopy model 2100F FEG-TEM (FEG: Field Emission Gun, USA) with an accelerator voltage of 200 kV was used to evaluate the microstructure of different nanocomposites in terms of dispersion and localization of D43B in the

PLA/plasticizer blends. The samples were molded in epoxy and cryo-microtomed at room temperature using an ultramicrotome Leica (model EMFC7, USA). The cut slices were 70 nm thick. The reported micrographs represent typical morphologies at least at four different locations.

2.3.5 | X-ray diffraction (XRD)

X- ray diffraction patterns for Dellite 43B and D43B-PLA/plasticizer systems were obtained using an X-ray diffractometer (type Bruker D8 Advance, USA) with a copper source (Cu), operated at 40 kV and 40 mA. The measurements were carried out in the range 1–40° of 2θ, and the distance between the clay mineral layer was calculated using the Bragg law.

2.3.6 | Differential scanning calorimetry (DSC)

Differential scanning calorimetry (DSC) was used to determine the thermal parameters of PLA, PLA/Plasticizer blends and D43-PLA/plasticizer nanocomposites. The measurements were carried out in a Q2000 (TA Instruments, USA) under a nitrogen atmosphere. First, the samples were heated from 20 to 200°C at a heating rate 10°C/min, followed by cooling to 20°C at a heating rate 20°C/min, and after by a second heating to 200°C at 10°C/min. Finally, a second cooling to bring the temperature within the apparatus to room temperature was performed.

2.3.7 | Oxygen and water vapor permeability

Oxygen transmission was measured using a MOCON Ox-Tran 2/20 (Minneapolis, USA) with an oxygen flow rate of 20 sccm, at 0% relative humidity, room temperature, and under atmospheric conditions. Minimum two tests were performed for each sample with a surface of 100 cm^2 and a thickness around 55 μm.

The water vapor transmission rate (WVTR) was also evaluated using Mocon PERMATRAN-W® Model 3/33, MG Plus master, standard water vapor permeation testing. Each film was analyzed in duplicate, according to standard ASTM F-1249-06 ($T = 38$, RH $= 100\%$).

2.3.8 | Traction tests

Tensile tests were performed to determine the mechanical behavior of D43B-PLA/plasticizer nanocomposites blown films. Testing was carried out on an Instron ElectroPlus E3000 testing machine with a 250 N load cell. The tensile modulus and elongation at break were measured at room temperature. The measurements were performed using a crosshead speed of 5 mm/min. The tested films samples had dimension of $20 \times 25.4 \times 0.06$ mm.

3 | RESULTS AND DISCUSSION

3.1 | Morphology

To investigate the phase morphology of PLA/plasticizer blends and of D43B-PLA/plasticizer nanocomposites, AFM observations on the fractured surfaces were performed (Figures 2 and 3). As shown in Figure 2, the addition of 5 wt% of plasticizers to the PLA induced two-phase systems with the plasticizer as dispersed phase. For PLA/PEO and PLA/PEG blends, PEO and PEG were dispersed in the form of uniform droplets in PLA matrix (Figure 2a,b). The spherical shape of the dispersed phase is more visible in the case of PLA/PEO (Figure 2b) than in the case of PLA/PEG (Figure 2b), thus suggesting that the nodules size in PEG are smaller than those in PEO. This difference can be related to the difference in molecular weight, where the PEG molecules have lower molecular weight than PEO and thus a much lower viscosity.[26] Similar structure was obtained for PLA/PCL blends. However, PCL particles showed an irregular shape corresponding to the typical structure of immiscible blends (Figure 2c).[27] Concerning PLA/AX89 system, as shown in Figure 2d, the interfacial phase separation between AX89 and PLA was very clear. The plasticizer AX89 was dispersed in continuous PLA phase in a sea-island type of structure.[28] This result confirmed the low interfacial adhesion between AX89 with PLA compared to PEO and PEG. Similar result was reported by Maroufkhani et al. (2018) in their study on the C10A-PLA/NBR nanocomposites.[29]

The addition of 3 wt% of D43B to PLA/plasticizer systems affected the morphology of the blends, except for the D43B-PLA/AX89 nanocomposite (Figure 3). In contrast to AX89, it proved challenging to distinguish the dispersed phase (PEO, PEG, and PCL) from the PLA phase in the other systems. This phenomenon can be attributed to the generation of a synergistic effect among D43B, PLA, and the plasticizers. This synergy resulted in an increased level of compatibility between PLA and the plasticizers. Indeed, the aromatic groups present in the D43B modifier had the potential to interact with the hydroxyl groups found in both these plasticizers and PLA chains, thereby promoting improved compatibility within the blend.[16,21,30,31]
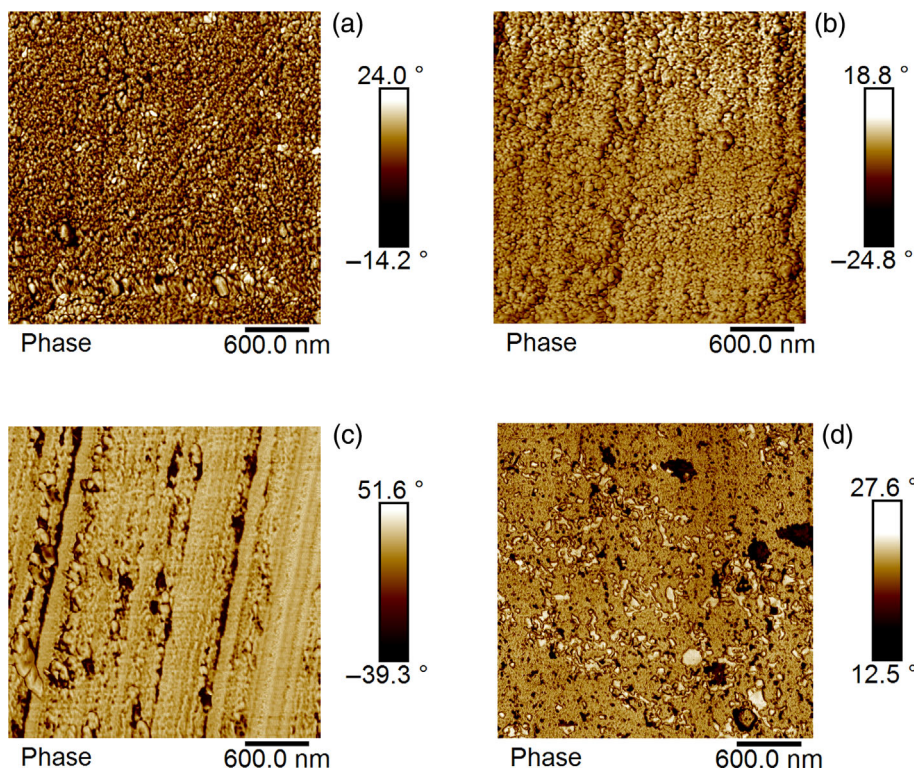
FIGURE 2 Atomic force microscopy (AFM) images of PLA/plasticizer films: (a) PLA/PEG; (b) PLA/PEO; (c) PLA/PCL, and (d) PLA/AX89. [Color figure can be viewed at wileyonlinelibrary.com]
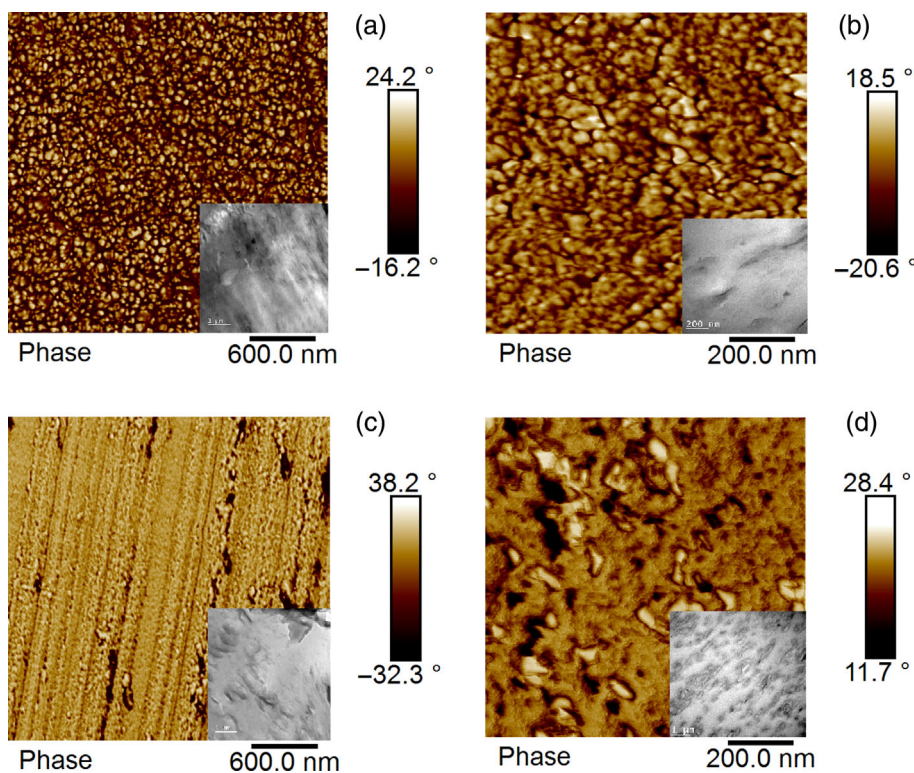

FIGURE 3 Atomic force microscopy (AFM) and transmission electron microscopy (TEM) images of D43B-PLA/plasticizer nanocomposites films: (a) D43B-PLA/PEG; (b) D43B-PLA/PEO; (c) D43B-PLA/PCL, and (d) D43B-PLA/AX89. [Color figure can be viewed at wileyonlinelibrary.com]

3.2 | Localization of OMMT PLA/plasticizer nanocomposite films

The estimated surface energies of the materials and the interfacial energies between the components at 23 and at 180°C are listed in Tables 2 and 3, respectively. PLA presented a surface energy at 31.69 ± 2.20 mN/m for a temperature of 23°C. Similar result was reported in the literature.[33,34] Concerning the plasticizers, PEO and AX89 shown surfaces energies lower than PLA. Unlike to

TABLE 2 Surface energies of PLA, plasticizers, and D43B at 23 and 180°C.

| | Surface tension (mN/m) | | | | | |
| | 23°C | | | 180°C | | |
	γ_s^p	γ_s^d	γ_S	γ_s^p	γ_s^d	γ_S
PLA	2.48 ± 0.30	29.20 ± 1.90	31.69 ± 2.20	1.88 ± 0.32	22.14 ± 2.04	24.03 ± 1.67
PEG	17.59 ± 0.42	41.87 ± 0.40	59.46 ± 0.82	15.30 ± 0.52	36.41 ± 0.49	51.71 ± 0.71
PEO	02.74 ± 0.18	25.91 ± 0.26	28.65 ± 0.43	2.01 ± 0.19	19.00 ± 0.27	21.01 ± 0.32
PCL	08.17 ± 0.15	29.92 ± 0.43	38.10 ± 0.58	6.52 ± 0.17	23.88 ± 0.49	30.40 ± 0.46
AX89	04.23 ± 0.27	23.85 ± 0.43	28.08 ± 0.70	3.40 ± 0.31	19.19 ± 0.49	31.73 ± 0.79
D43B	8.49 ± 0.28	30.94 ± 0.70	39.43 ± 0.98	5.24 ± 0.24	19.11 ± 0.61	24.35 ± 0.61
S43B	—	—	34.12a	—	—	21.08

aSurface tension of the organic modifier of D43B (S43B).[32]

TABLE 3 Interfacial energies between the components at 180°C.

| | Interfacial energies (mN/m) at 180°C | | |
| | Owens–Wendt model | | Girifalco–Good equation |
	PLA	D43B	S43B
PLA	—	0.98 ± 0.02	0.12 ± 0.15
PEG	8.26 ± 0.73	5.39 ± 0.06	6.76 ± 0.36
PEO	0.22 ± 0.01	0.76 ± 0.03	0.00 ± 0.00
PCL	1.47 ± 0.26	0.34 ± 0.03	0.85 ± 0.11
AX89	9.48 ± 0.39	9.33 ± 0.29	1.09 ± 0.21

PEO and AX89, higher values compared to the PLA were recorded by PCL and PEG. These findings can be attributed to the differences in the polarity of these compounds.[35] Essentially, a matrix with a greater number of polar groups in its chemical structure will exhibit higher surface energy, leading to the observed results.[18-20] At a temperature, the surface energy of various compounds decreased. This phenomenon can be attributed to the reduction of intermolecular cohesions due to increased thermal agitation at higher temperatures.[36] Regarding interfacial energies, Table 3 displays lower values for D43B-PLA, D43B-PCL and D43B-PEO when compared to D43B-PEG and D43B-AX89. This suggests a strong compatibility between D43B and PLA, and between D43B and PEO (PCL). However, D43B-PEG exhibited a lower interfacial energy compared to PEG–PLA, indicating better compatibility between PEG and D43B than between PLA and PEG. AS for AX89, the results obtained using the Girifalo-Good equation demonstrated a low interfacial energy between AX89 and the organic modifier of D43B. These results suggest the presence of compatibility between the organic modifier of D43B and AX89.

Obtained values for the spreading coefficient and the wetting parameter of D43B-PLA/plasticizer nanocomposites predicted that D43B should be located at the interface of PLA and plasticizers (Table 4). The value of wetting parameter for D43B-PLA/PEO nanocomposite is very close to 1, translating a better compatibility of this OMMt with PEO than with PLA. Unlike PEO, the system with AX89 as plasticizer showed a negative value close to −1, suggesting the high compatibility of D43B with PLA than with AX89.

To confirm the predictions obtained by the calculations of the spreading coefficient and wetting parameter, TEM observations were performed. As shown in Figure 4, the lighter sections represent the PLA matrix, whereas the small dark sections can be associated with the plasticizer as the dispersed phase, except in the case of D43B-PLA/PEG nanocomposite film where it is difficult to distinguish the dispersed phase from matrix phase. D43B is identified by fine black lines located in majority at the interface. The results obtained by TEM observations confirmed the previous results recorded by determination of the spreading coefficient and the wetting parameter, particularly for the case of D43B-PLA/PEO

	Spreading coefficient			Wetting parameter
	λ_{1S2}	λ_{S12}	λ_{12S}	ω_a
D43B-PLA/PEG	1.37 ± 0.22	-1.62 ± 0.51	-14.89 ± 0.94	-0.54 ± 0.043
D43B-PLA/PEO	0.02 ± 0.04	-0.27 ± 0.26	-1.49 ± 0.36	0.99 ± 0.005
D43B-PLA/PCL	0.49 ± 0.00	-0.74 ± 0.29	-9.11 ± 0.84	0.44 ± 0.085
D43B-PLA/AX89	8.27 ± 0.03	-8.51 ± 0.32	-8.49 ± 0.82	-0.88 ± 0.003

TABLE 4 The spreading coefficient and wetting parameter of the D43B-PLA/plasticizer nanocomposites.
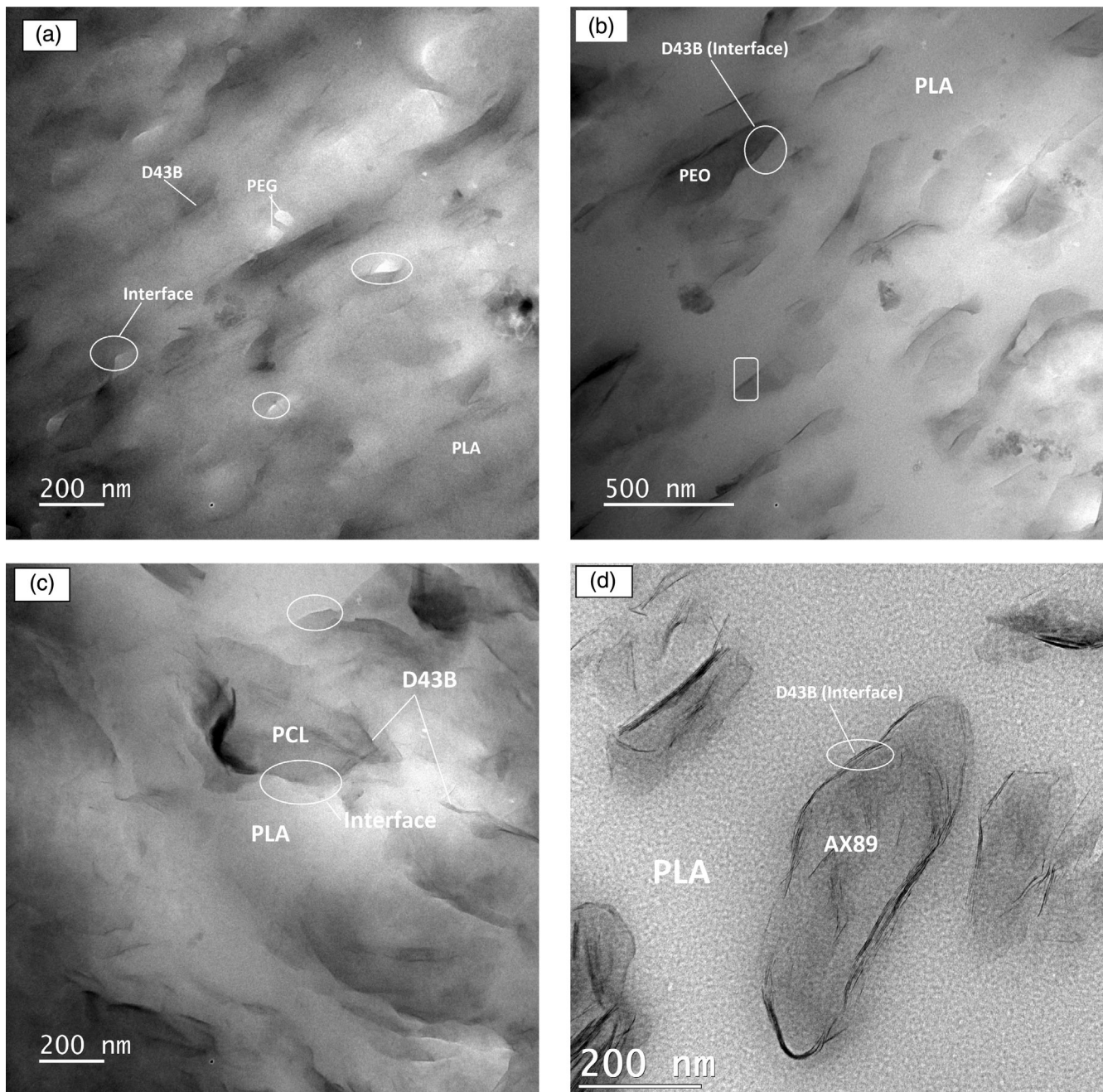
FIGURE 4 Transmission electron microscopy (TEM) images of D43B-PLA/plasticizer nanocomposites films: (a) D43B-PLA/PEG; (b) D43B-PLA/PEO; (c) D43B-PLA/PCL and (d) D43B-PLA/AX89 at 200–500 nm.

nanocomposite film (Figure 4(b)) where the OMMt was detected in the PEO phase. In the case of the D43B-PLA/AX89 nanocomposites, Figure 4(d) clearly depicts the presence of OMMt layers at the interface. However, the observation of some D43B layers within the AX89 phase suggests that D43B has not completely reached its thermodynamic equilibrium. This phenomenon can be explained by slow migration of OMMt toward its thermodynamically stable state, and the processing time applied during production is insufficient for its full migration to the interface. As result, OMMt become encapsulated within dispersed phase, which has a considerably lower melt temperature compared to the PLA matrix. This encapsulation occurs during the initial stages of the process when PLA, AX89 and D43B are mixed simultaneously. AX89, with its lower melt temperature encapsulates the D43B before PLA. A similar result was reported by Maroufkani et al. (2018) in their study on PLA/NBR nanocomposites using OMMt with the same surfactant as D43B.[29] However, the melting temperature of NBR (108°C) is higher than the T_m of AX89 (65°C), thus suggesting that OMMt will achieved it thermodynamic equilibrium faster with NBR than that with AX89.[4,17]

3.3 | OMMt dispersion in PLA/plasticizer nanocomposite films

To determine the dispersion status of D43B in PLA matrix with and without presence of 5 wt % of plasticizer, XRD measurements and TEM observations were performed. Figure 5 shows XRD patterns of D43B and D43B-PLA/plasticizer nanocomposite films, in the range 1–10°. D43B presents a characteristic diffraction peak at 4.8° corresponding to a basal distance (d_{001}) of 1.84 nm. Similar results were reported in literature.[37] The addition of 3 wt% of this OMMt into the PLA matrix resulted in a significant shift of its characteristic peak at a low angle, indicating the formation of an intercalated structure. Specifically, a peak at 2.66° corresponding to basal distance of 3.31 was observed. However, a small peak was also detected at $2\theta = 5.2°$, corresponding to a basal distance of 1.7 nm. This smaller peak could be attributed to a fraction characterized by a different arrangement of alkylammonium chains within the interlayer space.[38] In the case of D43B-PLA/plasticizer nanocomposite films, no significant changes were observed compared to D43B-PLA nanocomposite film. This suggests that the presence of 5 wt% of plasticizer in D43B-PLA nanocomposite film primarily affects the localization of D43B rather than its dispersion. These findings are further confirmed by TEM images presented in Figures 4 and 6. Moreover, in
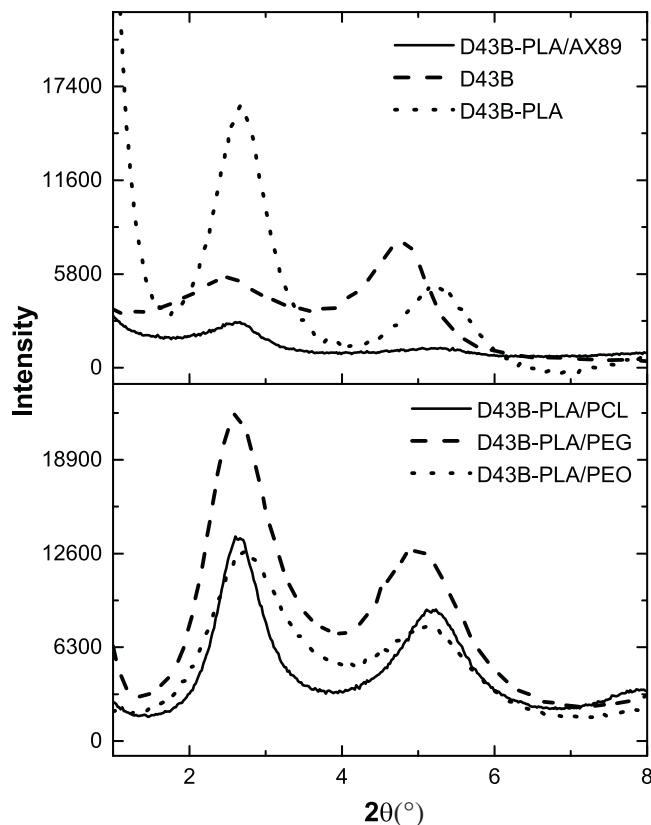

FIGURE 5 X-ray diffraction (XRD) patterns of D43B and D43B-PLA/plasticizer nanocomposites films, in the range 1–10°.

Figure 6, some black spots were observed, whish are believed to be agglomerations of the non-modified fraction of D43B.

3.4 | Thermal parameters of OMMt-PLA/plasticizer nanocomposites films

The thermal properties of the final films produced have a direct impact on their mechanical and barrier properties. It is important to note that crystallinity can undergo change during the extrusion-blowing process of film production. This phenomenon is significant because it has been reported in the literature that the effects of biaxial stretching, induced by the extrusion-blowing process, can influence the morphology and properties of clay/polymer nanocomposites. Indeed, the first heating cycle provides insight into the actual crystallinity of the film nanocomposites. During this initial heating phase, any crystals that formed during the film preparation process will undergo a melting transition. This melting of crystals is a significant event as it reveals the true assessment of its thermal and structural properties.[39,40] Figure 7 presents DSC thermograms of PLA and plasticizers at first
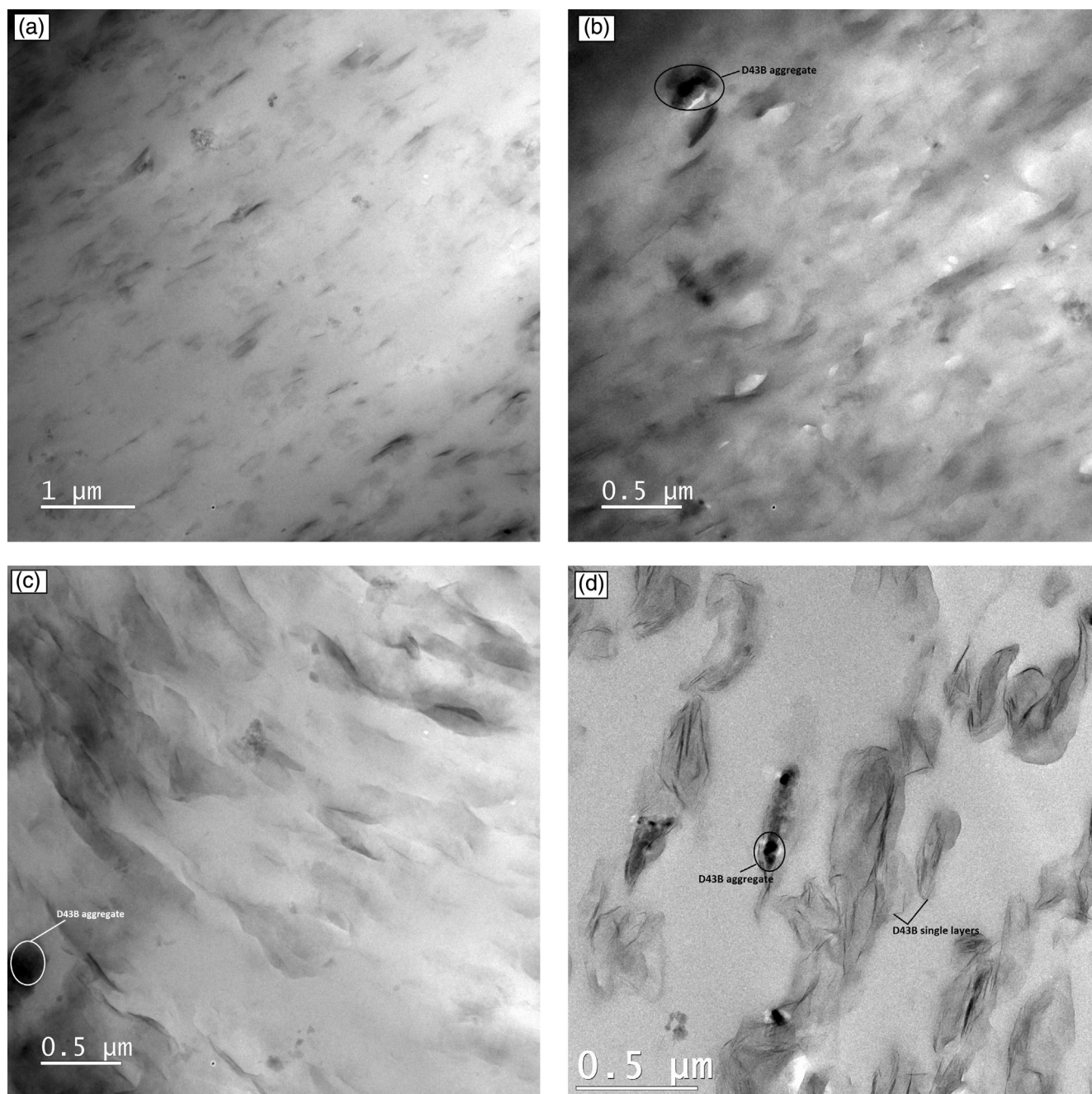
FIGURE 6 Transmission electron microscopy (TEM) images of D43B-PLA/plasticizer nanocomposites films: (a) D43B-PLA/PEO; (b) D43B-PLA/PEG; (c) D43B-PLA/PCL; and (d) D43B-PLA/AX89 at 0.5–1 μm.

heating. PEG, PEO, PCL and AX89 showed melt temperatures at 66, 65, 63 and 51–64°C, respectively, which coincide with the glass transition of PLA domains. PLA present a melt temperature (T_m) at 148°C and a glass transition temperature (T_g) at 64°C, which corroborate with the values found in literature.[41]

The thermal parameters of PLA/plasticizer blends and OMMt-PLA/plasticizer nanocomposite films are listed in Table 5. It is noteworthy that the glass transition temperature (T_g) of PLA exhibited a decrease following the addition of 5 wt% of plasticizer. This result can be attributed to the heightened chain mobility of PLA brought about by the insertion of plasticizer chains between the PLA chains. This insertion leads to the replacement of the original PLA–PLA homogeneous physical interactions with PLA-plasticizer hetero-phase interactions.[12,32] A reduction of 13°C of T_g was obtained with the PLA/PEG films, compared to the others PLA/plasticizer films. This can be associated to the lower molecular weight of PEG that facilitates its

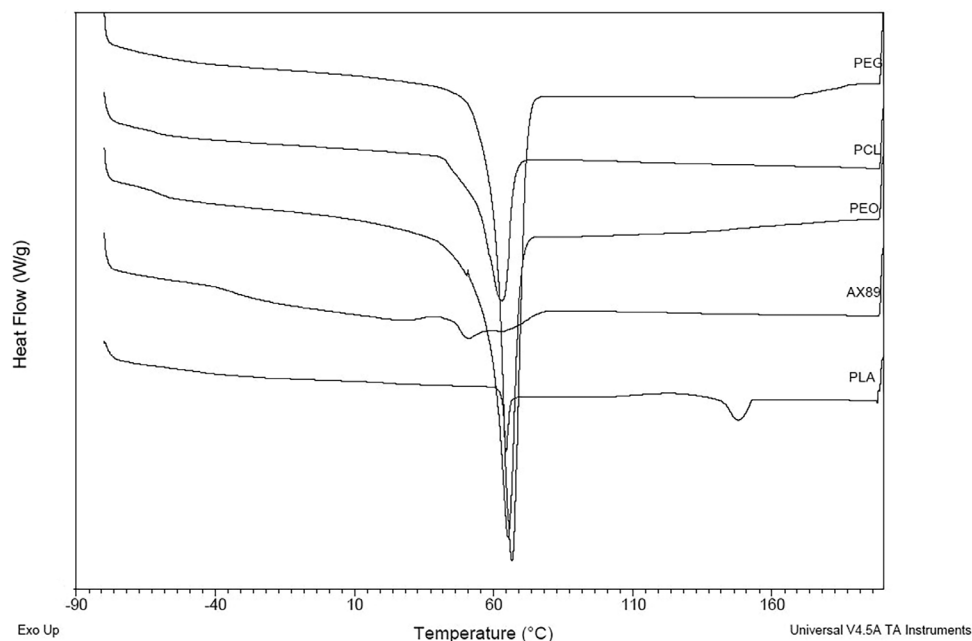**FIGURE 7** Differential calorimetric (DSC) thermograms of: PLA, PEG, PEO, PCL, and AX89 at first heating.

TABLE 5 Thermal parameters of PLA, PLA/plasticizer blends and OMMt-PLA/plasticizer nanocomposite films.

	First heating					
	T_g(PLA) (°C)	T_m (°C)	T_{cc} (°C)	ΔH_m (J/g)	ΔH_{cc} (J/g)	χ_c (J/g)
PLA	64	148	123	05.73	04.60	1.22
PLA/PEO	59	145	104	21.30	14.03	8.22
		149				
PLA/PEG	51	144	101	19.68	11.74	8.90
		149				
PLA/PCL	59	148	120	08.89	06.25	2.98
PLA/AX89	58	147	117	16.65	14.06	2.93
D43B-PLA	60	148	122	18.02	12.18	6.47
D43B-PLA/PEO	56	145	106	26.58	18.63	9.29
		149				
D43B-PLA/PEG	50	144	101	20.77	14.29	7.60
		151				
D43B-PLA/PCL	61	148	115	17.60	13.46	4.68
D43B-PLA/AX89	58	149	122	10.87	09.55	1.54

accommodation between the chains segment obstructing the tortuous path.[26] For D43B-PLA/plasticizer nanocomposite films, no significant change in T_g was observed compared to the PLA/plasticizer films. Similar results were reported in literature.[26–28] Similar to T_g, the cold crystallization peak temperature (T_{cc}) was also decreased after addition of 5 wt% of plasticizer.

The crystallinity rate X_C of different films produced, is calculated using the Equation 8, where the $\Delta H_m^0 = 93,0 J/g$[21] and W_{PLA} are respectively the enthalpy

for PLA 100% crystallin and its weight percentage in the PLA mixtures.

$$X_C(\%) = \frac{\Delta H_m - \Delta H_{cc}}{(W_{PLA})\Delta H_m^0} \times 100. \tag{8}$$

In the case of PLA/PEG and PLA/PEO films, a marked enhancement in the crystallinity rate was observed compared to films containing PCL and AX89. These findings support the notion of increased chains
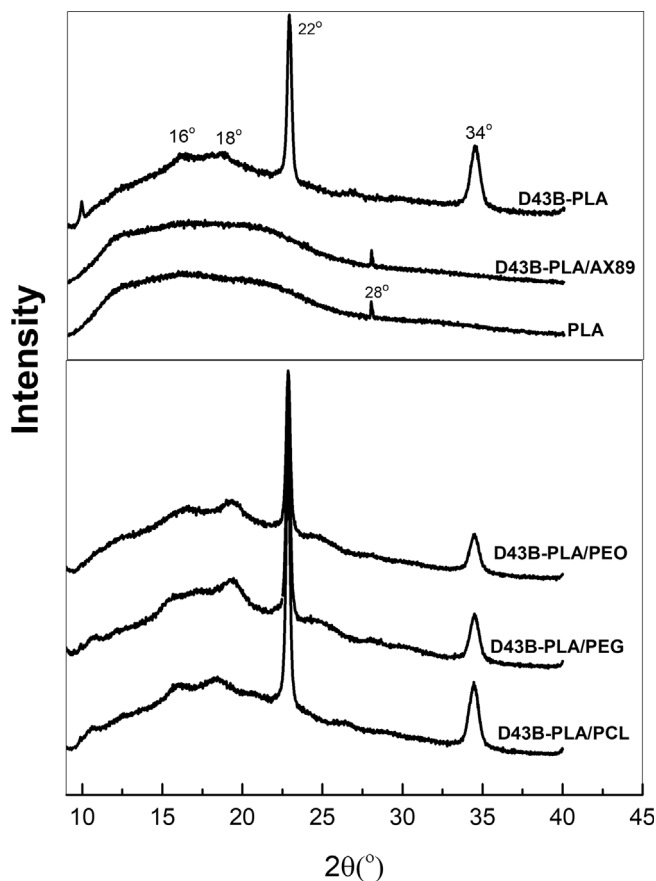
FIGURE 8 X-ray diffraction (XRD) patterns of PLA, D43B-PLA, and D43B-PLA/plasticizer nanocomposites films, in the range 10–40°.

mobility within PLA, which is responsible for the appearance of a second melting temperature around 144°C.[42] These results corroborate those reported by XRD (Figure 8). In Figure 8, it is evident that the D43B-PLA nanocomposite film exhibited distinct peaks at $2\theta = 16°(110), 18°(0010)$ and $22°(0010)$, which correspond to the characteristic diffraction peaks of the crystalline α-phase. Additionally, a characteristic peak of crystalline β-phase was observed at $2\theta = 34°$.[43] These results provide further confirmation of the effectiveness of D43B as nucleating agent. It appears that D43B induces a partial transformation of crystalline α'-phase to crystalline α-phase, while also promoting the formation of a fraction of crystalline β-phase. This nucleating efficacity can be associated to the high compatibility of D43B with the PLA matrix.

The simultaneous mixing of D43B, plasticizer and PLA matrix, showed an increase of crystallinity with PCL and with PEO nanocomposites. However, for the D43B-PLA/PEG nanocomposite film, a slight decrease in crystallinity was observed compared to the PLA/PEG film. This observation ca be related to the high interfacial

energy between D43B and PEG, indicating lower compatibility compared to the interaction between PEO and D43B. This confirmed the results obtained by calculations of wetting parameter, spreading coefficient and TEM images. Unlike to these plasticizers, the presence of AX89 in the D43B-PLA nanocomposite reduced the crystallinity. The encapsulation of D43B in the dispersed phase AX89 reduced its interactions with PLA matrix, with which it is more compatible. The results presented in Figure 8, confirm those shown by DSC analysis. Indeed, the peaks observed in the case of D43B-PLA nanocomposites that translated a change in the crystalline phases of PLA, were also recorded for all D43B-PLA/plasticizer nanocomposites films, except with AX89.

3.5 | Barrier properties of OMMt-PLA/plasticizer nanocomposite films

The permeability of water vapor (WVP) and oxygen in food packaging can drastically affect the quality of food and its shelf life.[38] Most biodegradable polyesters, particularly PLA, present poor barrier properties, particularly to oxygen.[44] To improve these properties, some additives such as plasticizers or OMMt are used to increase the crystallinity[41] or create a tortuosity effect,[15] respectively. Table 6 presents the WVP and oxygen permeability of PLA, PLA/plasticizer films and D43B-PLA/plasticizer nanocomposite films. A reduction of more than 20% of oxygen permeability in PLA film was obtained after the introduction of 5 wt% of plasticizers, particularly with PEG. The good oxygen barrier effect obtained in the case of PLA/PEO and PLA/PEG films can be related to the important increase in the crystallinity of PLA following to the addition of these plasticizers. While, the decrease of oxygen permeability recorded by for PLA/PCL and PLA/AX89 can be associated to the little increase of crystallinity and also to the polarity. Indeed, a high polarity translate a high cohesive energy density.[45] It was reported in literature that the oxygen permeability of a polymer decreased when the cohesive energy density increase.[45] The polarity (x_p) of PLA, PCL and AX89 are 0.078, 0.15 and 0.21, respectively. It was determined using the results obtained by the determination of surface tension, where $x_p = \gamma^p/\gamma$[50]. The presence of PCL and AX89 in the PLA matrix affected it polarity which induced an increased cohesive energy density of PLA, thus decreasing its oxygen permeability. Similar to the plasticizers, a reduction in the oxygen permeability of PLA was obtained after the incorporation of 3 wt% of D43B. However, the high compatibility of this OMMt with PLA matrix resulted in a better improvement of oxygen barrier compared to the plasticizers. The presence of D43B in

TABLE 6 Oxygen and the water permeability of PLA, PLA/plasticizer films, D43-PLA/plasticizer nanocomposites films.

	Oxygen permeability (cc·mil·m^{-2}·day^{-1}·atm^{-1})	Water vapor permeability (g·m^{-2}·day^{-1}·atm^{-1})
	$S = 100$ cm^2, RH = 0%, and $T = 23°$C	$S = 5$ cm^2, RH = 100% and $T = 38°$C
PLA	1102 ± 61	164 ± 11
PLA/PEO	734 ± 27	223 ± 01
PLA/PEG	621 ± 21	278 ± 16
PLA/PCL	809 ± 01	164 ± 02
PLA/AX89	854 ± 31	207 ± 17
D43B-PLA	478 ± 60	141 ± 39
D43B-PLA/PEO	632 ± 48	174 ± 02
D43B-PLA/PEG	598 ± 31	258 ± 05
D43B-PLA/PCL	560 ± 20	110 ± 01
D43B-PLA/AX89	995 ± 20	177 ± 12

PLA/plasticizer films improved its oxygen barrier, except for AX89. The encapsulation of D43B in AX89 phase reduced the polarity effect of this plasticizer and the compatibility between PLA and D43B. Unlike oxygen permeability, WVP was increased except for PCL where no change was observed. PEO and PEG presented high hydrophilicity (they are water soluble) compared to PLA, which favored the diffusivity and solubility of water molecules inside PLA/PEO (PEG) films.[39] For PLA/AX89 system, the increase of WVP can be related to the high interfacial energy between PLA and AX89, translating a poor compatibility. Unlike PLA/plasticizer films, D43B-PLA nanocomposites presented a reduction in WVP and oxygen permeability. This can be related to the high compatibility of D43B with PLA, which induced an increase in crystallinity and created the tortuosity effect. The presence of this OMMt on the PLA/plasticizer films induced to a decrease in the WVP. The reduction can be associated to the tortuosity effect induced by D43B.

3.6 | Mechanical properties of OMMt-PLA/plasticizer nanocomposite films

Tensile tests were performed on PLA, PLA/plasticizer, and D43B-PLA/plasticizer films, in the machine direction (Figures 9 and 10). PLA is a brittle polyester that has a high tensile modulus and low elongation at break.[11,17,46]

The addition of 5 wt% of plasticizer to the PLA was induced to a decrease in tensile modulus and an increase in the elongation at break. In the case of PLA/PEO film a significant improvement of elongation at break was obtained compared to PLA/PEG. The difference can be attributed to the difference in the molecular weight of these plasticizers. PEO with high molecular weight is
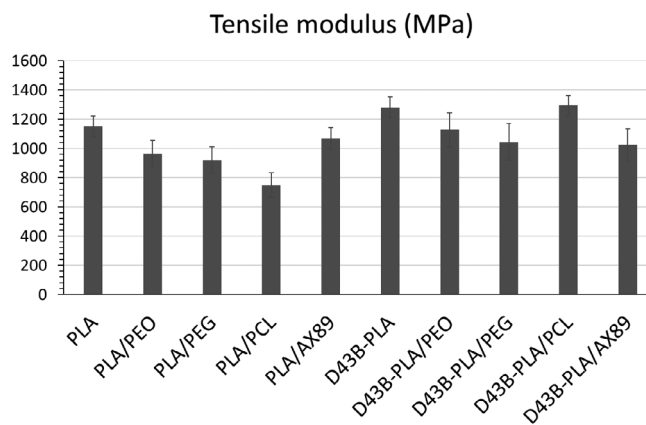

FIGURE 9 Tensile modulus of: PLA, D43B-PLA, PLA/plasticizer and D43B-PLA/plasticizer films.

more effective at increasing the elongation at break of PLA compared to lower molecular weight of PEG. Furthermore, the reduction of over 20% in oxygen permeability in PLA/PEG films, despite the low impact on the elongation at break, can be attributed to the dual nature of PEG. PEG, a hydrophilic polymer, enhance barrier properties by obstructing the diffusion of oxygen molecules through the film. However, the lack of a significant effect on the elongation at break suggests that the plasticizing effect of PEG may have been counteracted by others factors, such as the high interfacial energy between PEG and PLA and/or the effect from the processing conditions that were used in this study (process in two 2 steps). The exposure of PEG to high temperature for prolongate period, can induce to PEG molecules migration to the film's surface, inducing a reduction in the concentration of PEG within the bulk of the film, thus a decrease on its plasticizing impact. Similar to the PEO, a great improvement of the elongation at break was
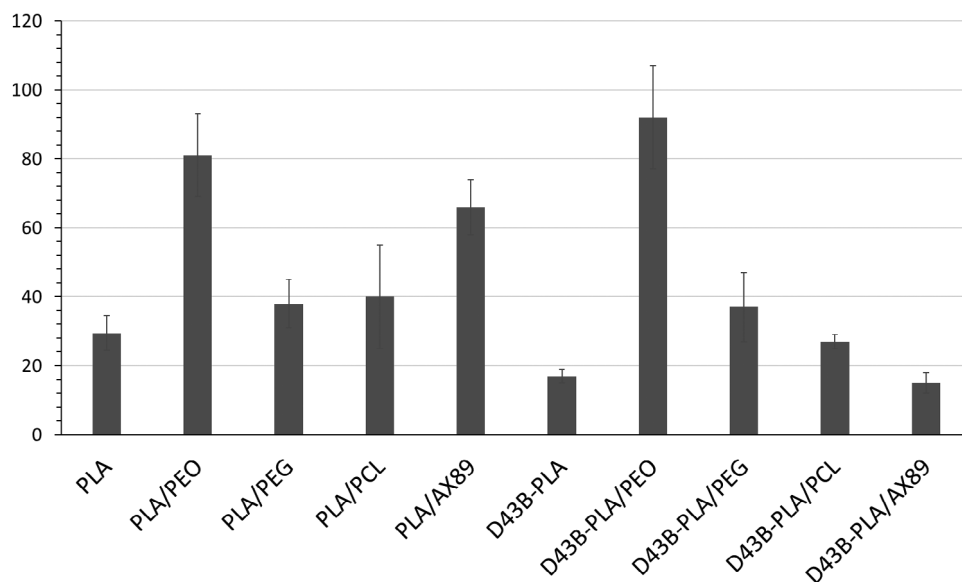
FIGURE 10 Elongation at the break of: PLA, D43B-PLA, PLA/plasticizer and D43B-PLA/plasticizer films.

obtained by PLA/AX89 film. This increase can be related to the structure of the AX89 plasticizer. In fact, the random arrangement of the three monomers (ethylene, methyl acrylate, and glycidyl methacrylate) along the polymer chain results in a less crystalline, more amorphous structure. This reduced crystallinity enhances ductility by allowing the chains to move freely and stretch.[47] The lower effect of PCL on the elongation at the break of PLA can be related to lower concentrations. Indeed, in literature, it was reported that a marked improvement can be observed from a concentration ≥20 wt% with PCL.[9,48] Unlike plasticizers, the incorporation of D43B into PLA results in an increased tensile modulus and decreased elongation at break. These effects were attributed to clay reinforcement, improved dispersion, reduced polymer chain mobility due to the high compatibility of D43B with PLA matrix.

Regarding the D43-PLA/plasticizer nanocomposites, a notable change in elongation at break was observed when compared to PLA/plasticizer system. Specifically, a significant increase was achieved in the case of the D43-PLA/PEO nanocomposite, indicating improved stretchability, while a decrease was noted in the case of D43B-PLA/PCL(AX89) nanocomposites, possibly due to the differing interaction and compatibility between the components in these nanocomposite systems. The remarkable compatibility observed between D43B, PLA matrix, and PEO, as evidenced by the wetting parameters, the spreading coefficients and TEM analysis, highlight the synergistic potential of these materials in nanocomposite formulations. This compatibility is a critical factor in the significant increase in elongation at break observed in the D43B-PLA/PEO nanocomposite.

The enhanced stretchability achieved in this system can be attributed to the harmonious interaction between D43B, PLA, and PEO, which facilitates the material's ability to deform before breaking. In contrast, the absence of this synergistic effect in the case of D43B-PLA/PEG resulted in no significant change in the elongation at break when compared to the PLA/PEG film. This discrepancy underscores the importance of specific material interactions in nanocomposite design. While D43B exhibited compatibility with PLA and PEO, this compatibility did not extend to PEG, leading to different mechanical properties. In the case of D43B-PLA/PCL nanocomposites, the concentration of PCL was found to be insufficient to exert a substantial impact on the elongation at break of PLA. For D43-PLA/AX89 nanocomposite, the encapsulation led to a decrease in compatibility between D43B and the PLA matrix. Consequently, the plasticizing effect of AX89 on the PLA matrix was significantly reduced, resulting in a decreased elongation at break.

4 | CONCLUSION

In conclusion, AFM observations showed distinct phase morphologies in PLA/plasticizer blends, with PEO and PEG forming uniform droplets, PCL displaying irregular shapes, and AX89 showing interfacial separation. The introduction of D43B improved compatibility in most cases, except in D43B-PLA/AX89.

Interfacial energy calculations and wetting parameter analysis confirmed strong compatibility between D43B and PLA, and PEO(PCL). D43B-PEG exhibited superior

compatibility to PEG–PLA. TEM observations supported these findings. X-ray analysis revealed intercalation in PLA with 3 wt% D43B, while 5 wt% plasticizer affected D43B's localization.

Plasticizers reduced the PLA's T_g and influenced crystallinity rates differently. D43B acted as a nucleating agent, except when combined with AX89. Plasticizers and OMMt enhanced barrier properties through compatibility, crystallinity, and polarity effects. D43B-PLA/plasticizer nanocomposites reduced oxygen permeability, except in case of D43B-PLA/AX89 due to encapsulation effect.

Regarding mechanical properties, PEG and PEO increased ductility and reduced oxygen permeability, with PEO performing better, due to its higher molecular weight. PLA/AX89 films improved elongation at break. D43B increased tensile modulus but reduced elongation at break. D43B-PLA/PEO exhibited remarkable elongation. Limited compatibility in D43B-PLA/PEG and reduced plasticizing effects in D43B-PLA/AX89 led to varied mechanical properties, emphasizing material interactions' role.

These findings have potential for food packaging materials but emphasize the balance between plasticizer effects, compatibility, and material interactions. Careful consideration of material combinations is essential for optimizing PLA-based nanocomposites in food packaging.

In conclusion, this research offers insights into PLA-based nanocomposite films for food packaging but underscores the need for thoughtful material selection to achieve the desired barrier and mechanical properties.

AUTHOR CONTRIBUTIONS
Salima ADRAR: Formal analysis (lead); methodology (equal); writing – original draft (equal); writing – review and editing (equal). **Abdellah Ajji:** Formal analysis (supporting); methodology (supporting); supervision (lead).

CONFLICT OF INTEREST STATEMENT
The authors declare no competing interests.

DATA AVAILABILITY STATEMENT
All data supporting the findings of this study are included in the article.

ORCID
Salima Adrar https://orcid.org/0000-0002-0251-9127

REFERENCES
[1] T. Saha, M. E. Hoque, T. Mahbub, *Advanced Processing, Properties, and Applications of Starch and Other Bio-Based Polymers*, Elsevier, London **2020**, p. 197. https://doi.org/10.1016/B978-0-12-819661-8.00013-5

[2] T. Z. Jin, L. Liu, in *ACS Symposium Series* (Eds: M. H. Tunick, L. Liu), American Chemical Society, Washington, DC **2020**, p. 83. https://doi.org/10.1021/bk-2020-1347.ch005

[3] C. Aversa, M. Barletta, A. Gisario, E. Pizzi, R. Prati, S. Vesco, *J. Appl. Polymer Sci* **2021**, *138*, 51294.

[4] Y. Ding, W. Feng, B. Lu, P. Wang, G. Wang, J. Ji, *Polymer* **2018**, *146*, 179.

[5] M. Bijarimi, S. Ahmad, R. Rasid, M. A. Khushairi, M. Zakir, *AIP Conference Proceedings*, AIP Publishing, Oludenzi **2016**.

[6] Y. Eom, B. Choi, S. Park, *J. Polym. Environ.* **2019**, *27*, 256.

[7] I. Fortelny, A. Ujcic, L. Fambri, M. Slouf, *Front. Mater.* **2019**, *6*, 206.

[8] S. Adrar, A. Habi, A. Ajji, Y. Grohens, *Appl. Clay Sci.* **2018**, *157*, 65.

[9] Y. Jiang, C. Yan, K. Wang, D. Shi, Z. Liu, M. Yang, *Materials* **2019**, *12*, 1663.

[10] M. Baiardo, G. Frisoni, M. Scandola, M. Rimelen, D. Lips, K. Ruffieux, E. Wintermantel, *J. Appl. Polym. Sci.* **2003**, *90*, 1731.

[11] S. Sharma, A. A. Singh, A. Majumdar, B. S. Butola, *Composites, Part B* **2020**, *188*, 107845.

[12] S. H. Othman, H. N. Ling, R. A. Talib, M. N. Naim, N. P. Risyon, M. Saifullah, *J. Nano Res* **2019**, *59*, 77.

[13] A. H. Mohsen, N. A. Ali, *J. Biorem. Biodegrad.* **2018**, *9*, 455.

[14] R. N. Darie, E. Pâslaru, A. Sdrobis, G. M. Pricope, G. E. Hitruc, A. Poiată, A. Baklavaridis, C. Vasile, *Ind. Eng. Chem. Res.* **2014**, *53*, 7877.

[15] S. Singha, M. S. Hedenqvist, *Polymers* **2020**, *12*, 1095.

[16] S. Marano, E. Laudadio, C. Minnelli, P. Stipa, *Polymer* **2022**, *14*, 1626.

[17] A. K. Mohapatra, S. Mohanty, S. k. Nayak, *Polym. Compos.* **2014**, *35*, 283.

[18] M. L. Iglesias-Montes et al., *Polymers* **2022**, Accessed: September 24, 2023 , *14*, 3177.

[19] E. Garofalo, L. Di Maio, P. Scarfato, P. Russo, L. Incarnato, *J. Polym. Environ.* **2023**, *31*, 4546.

[20] C. Alpaslan Güler, S. Deniz, *J. Dispersion Sci. Technol.* **2023**, *44*, 1.

[21] S. Adrar, A. Ajji, *Polym. Eng. Sci.* **2022**, *62*, 3796.

[22] J. Zhou, B. G. Min, *Fibers and Polymers* **2013**, *14*, 518.

[23] M. Lewin, A. Mey-Marom, R. Frank, *Polym. Adv. Technol.* **2005**, *16*, 429.

[24] A. D'Anna, R. Arrigo, A. Frache, *J. Polym. Environ.* **2022**, *30*, 102.

[25] M. Nofar, R. Salehiyan, S. S. Ray, *Composites, Part B* **2021**, *215*, 108845.

[26] D. Saha, S. K. Samal, M. Biswal, S. Mohanty, S. K. Nayak, *Polym. Int.* **2019**, *68*, 164.

[27] Y. Zhou, P. Wang, G. Ruan, P. Xu, Y. Ding, *ES Mater Manuf* **2021**, *11*, 20.

[28] G. F. Brito, P. Agrawal, E. M. Araujo, T. J. Melo, *Polym. Eng. Sci.* **2014**, *54*, 1922.

[29] M. Maroufkhani, A. Katbab, J. Zhang, *Polym. Test.* **2018**, *65*, 313.

[30] M. R. Rahnama, M. Barikani, M. Barmar, H. Honarkar, *Polym.-Plast. Technol. Eng.* **2014**, *53*, 801.

[31] C.-G. Sanporean et al., *RSC Adv.* **2014**, *4*, 6573.

[32] M. Yousfi, J. Soulestin, B. Vergnes, M.-F. Lacrampe, P. Krawczak, *Macromol. Mater. Eng.* **2013**, *298*, 757.

[33] T. Nazari, H. Garmabi, *Polym. Int.* **2018**, *67*, 178.

[34] M. R. Aghjeh, Y. Kazerouni, M. Otadi, H. A. Khonakdar, S. H. Jafari, H. Ebadi-Dehaghani, S. H. Mousavi, *Composites, Part B* **2018**, *137*, 235.

[35] S. Wu, in *Polymer Blends* (Eds: D. R. Paul, S. Newman), Academic Press, London **1978**, p. 243. https://doi.org/10.1016/B978-0-12-546801-5.50012-8

[36] G. Lefebvre, Modification de surface de particules de talc par de la silice nanométrique hydrophobe (par enrobage à sec): influence sur leurs propriétés physico-chimiques et leur dispersibilité dans une phase aqueuse. PhD Thesis, 2010.

[37] A. Araújo, G. Botelho, M. Oliveira, A. V. Machado, *Appl. Clay Sci.* **2014**, *88–89*, 144.

[38] M. Ramos, A. Jiménez, M. Peltzer, M. C. Garrigós, *Food Chem.* **2014**, *162*, 149.

[39] P. Ghosh, *Colloid and Interface Science*, PHI Learning Pvt. Ltd., New Delhi **2009**.

[40] L. Makkonen, J. Kurkela, *J. Colloid Interface Sci.* **2018**, *529*, 243.

[41] M. Cocca, M. L. Di Lorenzo, M. Malinconico, V. Frezza, *Eur. Polym. J.* **2011**, *47*, 1073.

[42] F. Li, C. Zhang, Y. Weng, *ACS Omega* **2020**, *5*, 18675.

[43] M. L. Di Lorenzo, R. Androsch, *Polym. Int.* **2019**, *68*, 320.

[44] X. Chen, D. Xiang, Z. Zhou, Y. Wu, H. Li, C. Zhao, Y. Li, *Front. Mater* **2021**, *8*, 725422.

[45] A. Y. Alentiev, Y. P. Yampolskii, *J. Membr. Sci.* **2002**, *206*, 291.

[46] R. U. Rao, B. Venkatanarayana, K. N. S. Suman, *Mater. Today: Proc* **2019**, *18*, 85.

[47] Z. Cao, H. Pan, Y. Chen, L. Han, J. Bian, H. Zhang, L. Dong, Y. Yang, *Int. J. Biol. Macromol.* **2019**, *137*, 1141.

[48] S. Wu, *Polymer blends*, Elsevier, London **1978**, p. 243.